Supporting Information

In Situ Formation of Circular and Branched Oligomers in Localized High Concentration Electrolyte at Lithium−metal Solid Electrolyte Interphase: A Hybrid ab initio and Reactive Molecular Dynamics

*Yue Liu[a], Qintao Sun[a], Peiping Yu[a], Bingyun Ma[a], Hao Yang[a], Jiayi Zhang[a], Miao Xie[a], and Tao Cheng[a]**

[a] Institute of Functional Nano and Soft Materials (FUNSOM), Soochow University, Suzhou 215123, China

*To whom correspondence should be addressed.

E-mail: tcheng@suda.edu.cn; 0000-0003-4830-177X

Computational Details:

The highest occupied molecular orbital (HOMO) and lowest unoccupied molecular orbital (LUMO) shown in Figure 2 are obtained from calculations on isolated solvent, salt, and solvent+salt complex using Gaussian 16 under B3LYP level with 6-311+G* basis set. The red and green regions represent the positive and negative phases of the molecular orbitals, respectively. All molecular orbitals are shown with an isovalue of 0.03.

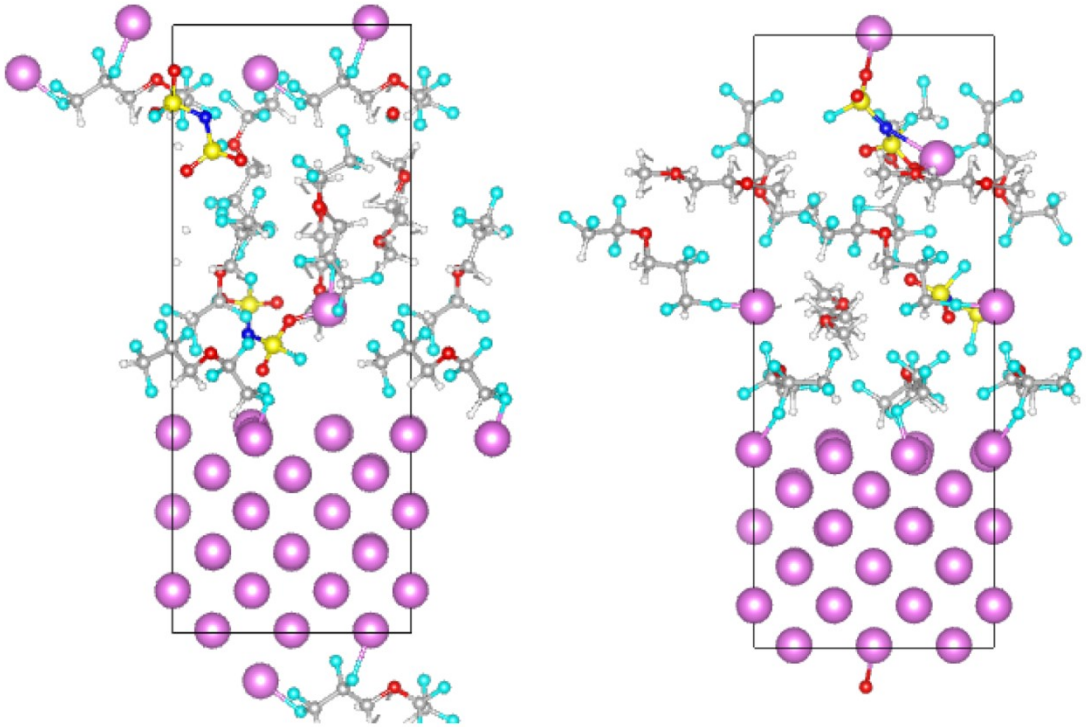

Figure S1. Initial configurations of lithium–metal anode surface and LiFSI/DME/TTE electrolyte. Color code: lithium, purple; oxygen, red; carbon, gray; fluorine, cyan; sulfur, yellow, nitrogen, blue; hydrogen, white.

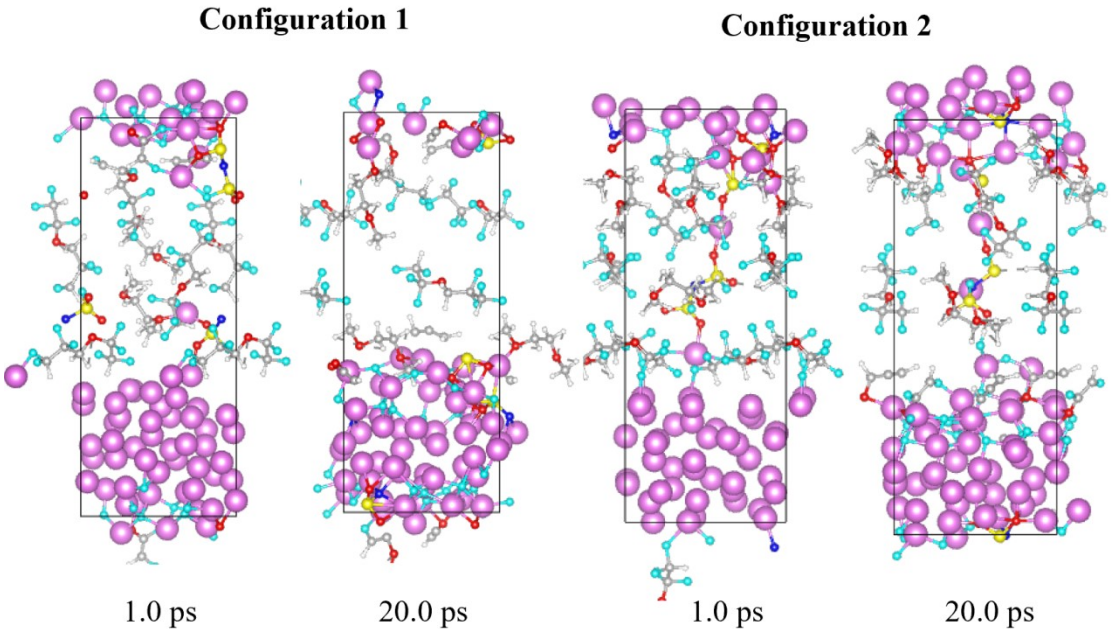

Figure S2. Snapshots of Li-metal anode and LiFSI/DME/TTE electrolyte (two configurations) at 1.0 ps and 20.0 ps in AIMD simulations. The color codes are the same as in Figure S1.

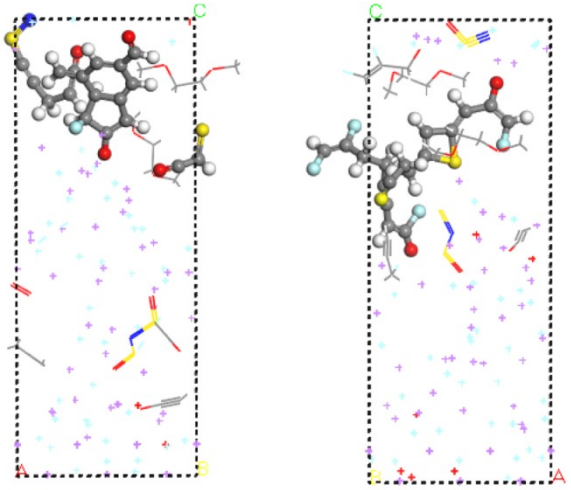

Figure S3. The polymer formed from two configurations after 275 ps (50 cycles) using HAIR MD simulation. The color codes are the same as in Figure S1.

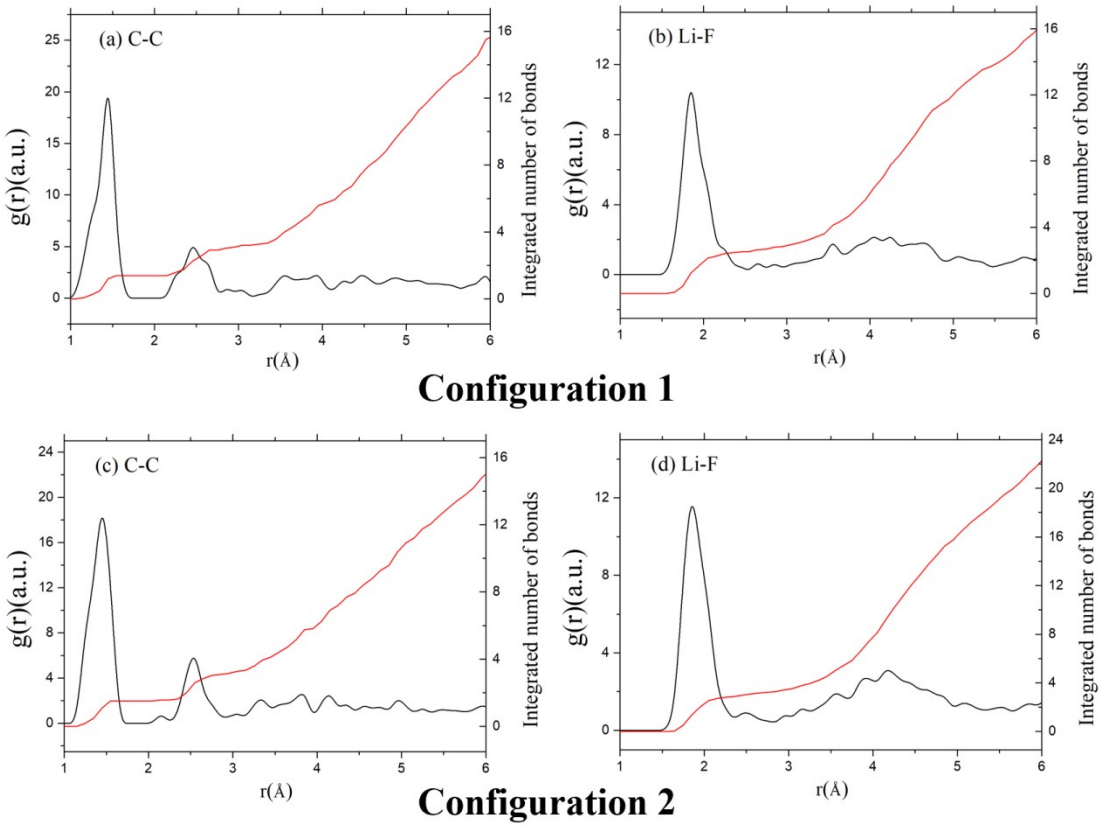

Figure S4. Radial distribution function and integrated number of bonds for (a) C-C; (b) Li-F for configuration 1 (c) C-C; (d) Li-F for configuration 2 after 2.85 ns HAIR simulations. The black line for radial distribution function, the red line for an integrated number of bonds.

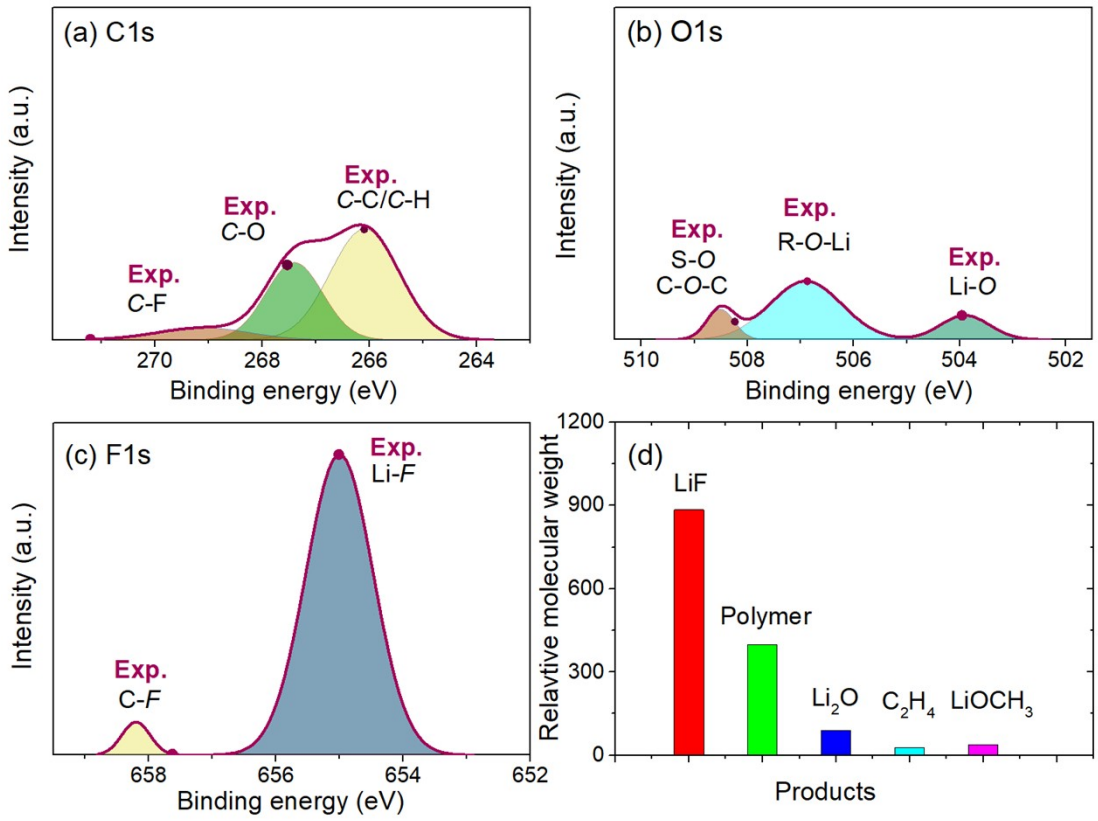

Figure S5. XPS spectra of configuration 2 for (a) C1s; (b) O1s; and (c) F1s. Exp. Represent the binding energy shifts, and the corresponding values are shown in Table S1-S3.

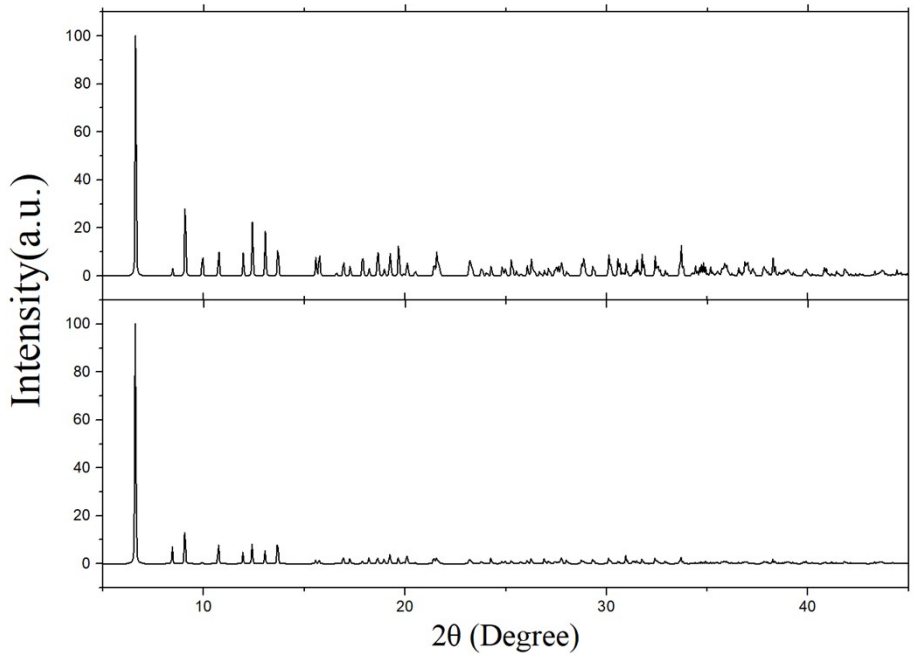

Figure S6. XRD patterns from MD simulations for two configurations.

Table S1. Experimental and theoretical C1s XPS binding energy (eV) and relative binding energy shift to C-C/C-H.

C1s	Exp.	Configuration 1	Configuration 2	Exp. shift	Configuration 1. shift	Configuration 2. shift
C-H/*C*-C	284.9	265.4	266.1	0	0	0
C-O	286.3	266.9	267.4	1.4	1.5	1.3
C=O	287.8	267.9	-	2.9	2.5	-
C-F	289.8	268.7	269.1	4.9	3.2	3
C-F_2	-	270.1	-	-	4.7	-

Table S2. Experimental and theoretical O1s XPS binding energy (eV) and relative binding energy shift to Li_2-O.

O1s	Exp.	Configuration 1	Configuration 2	Exp. shift	Configuration 1. shift	Configuration 2. shift
Li_2-*O*	528.2	503.7	503.9	0	0	0
R-*O*-Li/*O*-H	531.3	506.5	506.9	3.1	2.8	3
S-*O*/C-*O*-C	532.5	508	508.5	4.3	4.3	4.6

Table S3. Experimental and theoretical F1s XPS binding energy (eV) and relative binding energy shift to Li-F.

F1s	Exp.	Configuration 1	Configuration 2	Exp. shift	Configuration 1. shift	Configuration 2. shift
Li-*F*	684.7	655.4	655	0	0	0
C-*F*	687.3	658.1	658.2	2.6	2.7	3.2

Table S4. The Fermi energies of AIMD results at every five cycles interval

Serial number	Fermi energy (eV)	Serial number	Fermi energy (eV)	Serial number	Fermi energy (eV)
1	1.5763	9	-0.0112	17	-0.7762
2	1.5214	10	-0.4356	18	0.2114
3	1.057	11	-0.522	19	0.5126
4	0.5666	12	-0.2954	20	0.774

5	0.373	13	0.239	21	0.774
6	-0.4838	14	0.1103	22	1.1622
7	-0.8922	15	0.3114	23	1.4869
8	-0.7226	16	0.2426		

There are two methods to calculate the core-level shift-the initial and finial state approximation in VASP. The initial state approximation is based on Kohn-Sham (K.S.) eigenvalues of the core state after self-consistent calculation of the valence charge density, while the final state approximation relies on calculating the energy for a situation with one or one-half of an electron (employing Slater's transition state theory) excited from the core into the valence region[1-3]. Although using final state approximation usually can get the core level energy approachable with absolutely experimental binding energy, in our previous study and other theoretical studies, the core level energy shift would be fitted well with experimental binding energy shift in the initial state approximation[1,3,4]. And the binding energy shift is more important than binding energy values, especially in theoretical simulations and XPS (**Table S6**, which are 1.58 and 1.48 eV, respectively). And fixing one or one-half of an electron excited from the core into the valence region to get the core level energy would result in serious artifacts in the present case[3]. So, we selected the initial state approximation to calculate the core level energy and the core level energy shift and compared them with the corresponding binding energy and binding energy shift in the experiment.

Table S6. The binding energy shift to CO with an initial state and final state compared with experimental results.

Method	CO_2 (eV)	CO (eV)	Binding Energy shift to CO (eV)
Initial state	282.60	281.02	1.58
Final state	323.73	323.62	0.11
Experiment[4]	297.69	296.21	1.48

References

1. Qian, J.; Baskin, A.; Liu, Z.; Prendergast, D.; Crumlin, E. J., Addressing the sensitivity of signals from solid/liquid ambient pressure XPS (APXPS) measurement. *J. Chem. Phys.* **2020**, *153 (4)*, 044709.

2. Slater, J. C. Quantum Theory of Molecules and Solids; McGraw-Hill: **1974**; Vol. 4.

3. Taucher T. C.; Hehn I.; Hofmann O. T.; Zharnikov M.; Zojer E. Understanding Chemical versus Electrostatic Shifts in X-ray Photoelectron Spectra of Organic Self-Assembled Monolayers. *J. Phys. Chem. C* **2016**, 120, 6, 3428–3437.

4. Hao Yang, Fabio Ribeiro Negreiros, Qintao Sun, Miao Xie, Luca Sementa, Mauro Stener, Yifan Ye, Alessandro Fortunelli, William A. Goddard, and Tao Cheng. Predictions of Chemical Shifts for Reactive Intermediates in CO2 Reduction under Operando Conditions. *ACS Appl. Mater. Interfaces* **2021** *13(27)*, 31554-31560.